Membrane Biology:

A TRPV4 Channel C-terminal Folding Recognition Domain Critical for Trafficking and Function

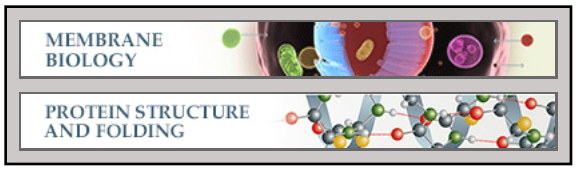

Lei Lei, Xu Cao, Fan Yang, Di-Jing Shi, Yi-Quan Tang, Jie Zheng and KeWei Wang

J. Biol. Chem. 2013, 288:10427-10439.
doi: 10.1074/jbc.M113.457291 originally published online March 2, 2013

THE JOURNAL OF BIOLOGICAL CHEMISTRY VOL. 288, NO. 15, pp. 10427–10439, April 12, 2013

A TRPV4 Channel C-terminal Folding Recognition Domain Critical for Trafficking and Function*

Received for publication, January 29, 2013, and in revised form, February 22, 2013 Published, JBC Papers in Press, March 2, 2013, DOI 10.1074/jbc.M113.457291

Lei Lei[‡], Xu Cao[‡], Fan Yang[§], Di-Jing Shi[‡], Yi-Quan Tang[‡], Jie Zheng[§1], and KeWei Wang[‡¶‖2]

From the [‡]Department of Neurobiology, Neuroscience Research Institute, Peking University Health Science Center, Beijing 100191, China, the [§]Department of Physiology and Membrane Biology, University of California School of Medicine, Davis, California 95616, the [¶]Department of Molecular and Cellular Pharmacology, State Key Laboratory of Natural and Biomimetic Drugs, Peking University School of Pharmaceutical Sciences, Beijing 100191, China, and the [‖]PKU-IDG/McGovern Institute for Brain Research, Peking University, Beijing 100871, China

Background: Overactive TRPV4 mutants cause human diseases, such as skeletal dysplasias.
Results: We identified C-terminal residues 838–857 to be critical for folding and surface expression, thus contributing to the regulation of channel activity.
Conclusion: Channels lacking the segment remain misfolded and are subjected to degradation via an ERAD-dependent pathway.
Significance: Targeting the folding recognition domain presents attractive therapeutic potential for overactive TRPV4-mediated pathology.

The Ca^{2+}-permeable transient receptor potential vanilloid subtype 4 (TRPV4) channel mediates crucial physiological functions, such as calcium signaling, temperature sensing, and maintaining cell volume and energy homeostasis. Noticeably, most disease-causing genetic mutations are concentrated in the cytoplasmic domains. In the present study, we focused on the role of the TRPV4 C terminus in modulating protein folding, trafficking, and activity. By examining a series of C-terminal deletions, we identified a 20-amino acid distal region covering residues 838–857 that is critical for channel folding, maturation, and trafficking. Surface biotinylation, confocal imaging, and fluorescence-based calcium influx assay demonstrated that mutant proteins missing this region were trapped in the endoplasmic reticulum and unglycosylated, leading to accelerated degradation and loss of channel activity. Rosetta *de novo* structural modeling indicated that residues 838–857 assume a defined conformation, with Gly^{849} and Pro^{851} located at critical positions. Patch clamp recordings confirmed that lowering the temperature from 37 to 30 °C rescued channel activity of folding-defective mutants. Moreover, biochemical tests demonstrated that, in addition to participating in C-C interaction, the C terminus also interacts with the N terminus. Taken together, our findings indicate that the C-terminal region of TRPV4 is critical for channel protein folding and maturation, and the short distal segment plays an essential role in this process. Therefore, selectively disrupting the folding-sensitive region may present therapeutic potential for treating overactive TRPV4-mediated diseases, such as pain and skeletal dysplasias.

TRPV4 (transient receptor potential vanilloid subtype 4) is a Ca^{2+}-permeable, non-selective cation channel that plays a critical role in maintaining cell volume and energy homeostasis (1–3). Like other members of the TRP channel superfamily, TRPV4 is a tetramer with the four subunits assembled in 4-fold symmetry surrounding a central ion permeation pore (4, 5). Each subunit contains six transmembrane segments (TM1–TM6)[3] with a pore-forming loop between TM5 and TM6 and both the N and C termini are located on the intracellular side (5, 6). Members of the TRPV subfamily share conserved structural elements, such as the N-terminal ankyrin repeat domain (ARD) and the C-terminal TRP-like box immediately after TM6 (5, 7, 8). The cryo-electron microscopy structure of TRPV4 at 3.5 nm resolution resembles a "hanging basket," with approximately 70% of the total volume being underneath the plasma membrane (9), indicating a role of the predominant intracellular portion of the channel in interacting with cytoplasmic proteins and modulating channel function. Consistent with the structural features, genetic analysis revealed that most naturally occurring TRPV4 mutations that lead to human diseases, such as metatropic dysplasia, are located in the cytoplasmic domains (10–12). Although it is known that many of these mutations lead to increased channel activity (10), no treatment to correct the overactive phenotype is currently available. Therefore, understanding how the mutation-prone cytoplasmic domains contribute to TRPV4 structural and functional properties has important implications for both fundamental understanding of physiology and pharmaceutical practice.

Among the homologous heat-sensitive TRPV1–4 channels, TRPV4 stands unique in that its major physiological function appears to be sensing physical stress, such as hypotonicity-induced cell swelling (2, 3, 13–17). TRPV4 is also uniquely sensi-

* This work was supported, in whole or in part, by National Institutes of Health Grant R01NS072377 (to J. Z.). This work was also supported by National Science Foundation of China Research Grants 30970919 and 81221002 (to K. W. W.); Ministry of Education of China, 111 Project China, Grant B07001; and Ministry of Science and Technology of China Grant 2013CB531300 (to K. W. W.).

[1] To whom correspondence may be addressed. Tel.: 530-7521241; Fax: 530-7525423; E-mail: jzheng@ucdavis.edu.

[2] To whom correspondence may be addressed. Tel.: 8610-82805065; Fax: 8610-82805065; E-mail: wangkw@bjmu.edu.cn.

[3] The abbreviations used are: TM, transmembrane segment; ARD, ankyrin repeat domain; ER, endoplasmic reticulum; ERAD, ER-associated protein designation; 2-APB, 2-aminoethoxydiphenyl borate; CHX, cycloheximide; EGFP, enhanced green fluorescent protein; CT, C terminus.

tive to a variety of chemical stimuli, including endocannabinoids, arachidonic acid metabolites, phorbol ester 4α-phorbol 12,13-dicaprinate, and synthetic compound GSK1016790A (18–21). TRPV4 is ubiquitously expressed in tissues, where its abundance at the cell surface is critical for regulating intracellular calcium signaling, temperature sensing, and osmo- and mechano-transduction as well as maintenance of cell volume and energy homeostasis (1, 22–24). Hence, the contribution of TRPV4 to its host cell physiology can be regulated and disturbed in human diseases through both the expression level and activity level (25–28).

The abundance of TRPV4 in cell surface depends on a complex series of events, from protein synthesis and proper folding in the endoplasmic reticulum (ER) to co- and post-translational modification, such as glycosylation and subunit assembly, before trafficking and targeting to the membrane surface as well as protein degradation (29). Maturation of TRP proteins requires ER-to-Golgi transport, characterized by transition from the *N*-linked high mannose glycosylation in the ER to the complex glycosylation in the Golgi apparatus (29). Dysfunctional TRP channels that fail to fold or assemble properly in the ER are usually characterized by a lack of complex glycosylation (29–32). The intracellular C-terminal region of TRPV4 has been shown to interact with various structural or modulatory proteins that regulate channel activity and surface expression, including MAP7, actin/tubulin, inositol trisphosphate receptor, TRPP2, and calmodulin (33–37). Fluorescence resonance energy transfer (FRET) and confocal imaging studies have attributed to the TRPV4 C terminus an important role in channel subunit oligomerization and trafficking (38, 39). However, despite the importance of TRPV4 in normal physiology and human genetic diseases, information regarding the underlying molecular mechanisms for TRPV4 trafficking and maturation as well as the role of the C terminus in these processes remains scarce.

In this study, we identified a novel segment comprising 20 amino acids in the distal C terminus of mouse TRPV4 (residues 838–857) that is critical for mediating protein folding and trafficking. TRPV4 channels lacking these residues remain misfolded and fail to reach the Golgi apparatus for complex glycosylation and maturation, and they are subjected to degradation through the ERAD-dependent pathway. Thus, we propose that selective disruption or inhibition of TRPV4 function by targeting this region may present therapeutic potentials for overactive TRPV4-mediated pathology, such as pain and skeletal dysplasias (23, 26, 40, 41).

EXPERIMENTAL PROCEDURES

Molecular Biology—The cDNAs of wild type (WT) mouse TRPV4 and its mutant forms were constructed by LA Taq (TAKARA) and inserted into either the vector pCDNA3.1(+) with three tandem-repeated FLAG epitopes (DYKDDDDK) at the N terminus for Western blot analysis or the vector pEGFPC2 (Clontech) for fluorescence microscopy. To facilitate functional tests, mutations were generated in the mutant TRPV4 background containing double mutations (N456H and W737R; named TRPV4dm) because these two mutations conferred 2-aminoethoxydiphenyl borate (2-APB) sensitivity. All restriction enzymes were purchased either from Invitrogen or Takara, and inserts of all cDNA clones were verified by sequencing.

Cycloheximide Treatment and Western Blotting Assay—For cycloheximide treatment, transiently transfected HEK293 cells were treated with cycloheximide for multiple time periods (as indicated in Fig. 3) and analyzed by Western blot. For Western blot assay, HEK293 cells were lysed in 100 μl of ice-cold lysis buffer Nonidet P-40 (50 mM Tris-HCl, 150 mM NaCl, 1% Nonidet P-40, 5 mM EDTA, pH 7.4) supplemented with protease inhibitor mixture (Roche Applied Science) for 30 min on ice. Cell lysates were then centrifuged at 4 °C for 20 min at 14,000 × *g*. Supernatants were loaded with 5× SDS-PAGE sample buffer, separated by SDS-PAGE, and transferred onto nitrocellulose membranes (Millipore). After blocking with the buffer of 5% powdered nonfat milk in TBS-T (Tris-buffered saline with 0.05% Tween 20), the membranes were incubated overnight at 4 °C with primary antibody (1:5000 for anti-FLAG from Sigma; 1:500 for anti-actin from Santa Cruz Biotechnology, Inc. (Santa Cruz, CA)), and immunoreactive bands were visualized by using the Immobilon Western HRP substrate (Millipore).

Confocal Fluorescence Microscopy—HEK293 cells were grown on coverslips at 37 °C under 5% CO_2 in DMEM supplemented with 10% fetal bovine serum. All transfections by cDNA constructs were made using Lipofectamine 2000 (Invitrogen), following the manufacturer's instructions. For confocal imaging, HEK293 cells were transfected with EGFP-tagged constructs. For localization in the ER, HEK293 cells were co-transfected with TRPV4dm-EGFP or mutant-EGFP and DsRed2-ER (Clontech). One day after transfection, HEK293 cells were washed three times in phosphate-buffered saline (PBS) and fixed with 4% paraformaldehyde in PBS for 15 min before being washed in PBS three times. Images were acquired using a confocal microscope (FV1000, Olympus).

Cell Surface Biotinylation Assay—Confluent monolayer HEK293 cells transfected with FLAG-TRPV4dm or FLAG-TRPV4dmΔ838–857 were washed three times with ice-cold Ca^{2+}/Mg^{2+}-PBS. Cells were biotinylated with 0.5 mg/ml sulfosuccinimidyl 2-(biotinamido)-ethyl-1,3-dithiopropionate (Pierce) in Ca^{2+}/Mg^{2+}-PBS at pH 7.4 and 4 °C for 30 min. The remaining biotin was quenched by incubating the cells for an additional 10 min with 100 mM glycine in TBS. Cells were then washed with PBS and lysed in ice-cold lysis buffer Nonidet P-40 with protease inhibitor mixture at 4 °C for 30 min and centrifuged at 14,000 × *g* for 10 min. One fraction of the cell lysate containing about 200 μg of proteins was incubated with 20 μl of neutravidin beads (Pierce) at 4 °C for 4 h, and the other fraction was prepared as total protein. After incubation, the beads carrying surface proteins were washed with buffer Nonidet P-40 and eluted with loading buffer. The total and surface proteins were both loaded onto 8% SDS-PAGE and assayed by Western blotting.

Endoglycosidase H and Peptide:N-Glycosidase F Digestion—20 μg of total proteins from HEK293 expressing FLAG-TRPV4dm or FLAG-TRPV4dmΔ838–857 were boiled for 10 min in the presence of 40 mM DTT and 0.5% SDS. Digestion was performed in a total volume of 30 μl with 2 μl (1000 units) of endoglycosidase H or peptide:*N*-glycosidase F (New England

Biolabs) at 37 °C for 2 h. Reactions were stopped by the addition of SDS-PAGE sample buffer and analyzed by Western blotting with anti-FLAG antibody as described above.

Electrophysiology—For whole-cell recording, patch pipettes were pulled from borosilicate glass and fire-polished to a resistance of ~2 megaohms. The recording pipette was filled with an internal solution containing 140 mM cesium aspartate, 3.5 mM NaCl, 0.3 mM $CaCl_2$, 0.3 mM Na_2GTP, 0.5 mM EGTA, 10 mM HEPES, 4 mM Mg-ATP (pH 7.3, adjusted with CsOH). Cells were initially perfused with a solution containing 110 mM NaCl, 1 mM $MgCl_2$,1 mM $CaCl_2$, 10 mM glucose, 10 mM HEPES (pH 7.3, adjusted with NaOH). Whole-cell currents were recorded using a HEKA EPC10 amplifier with PatchMaster software (HEKA). Membrane potential was held at 0 mV unless stated otherwise. During whole-cell recording, the capacity current was minimized by the amplifier circuitry, and the series resistance was compensated by 80%. The voltage ramp protocol was initiated by a voltage step to −100 mV for 10 ms, followed by a 400-ms ramp from −100 to 100 mV. The current was low pass-filtered at 2Hz and sampled at a 20-kHz rate.

Intracellular Calcium Measurement—Changes in intracellular calcium level ($[Ca^{2+}]_i$) in a population of cells were measured by fluorescent calcium-sensitive dyes in the Calcium 5 Assay Kit using a FlexStation 3 Microplate Reader (Molecular Devices). HEK293 cells were seeded at a density of ~30,000 cells/well in 96-well black-walled plates (Thermo) covered with poly-D-lysine. Cells were transfected with TRPV4dm or deletion mutants and grown overnight at either 37 or 30 °C. Cells were loaded with the FLIPR Calcium 5 Assay Kit for 1 h at 37 or 30 °C in the presence of 2.5 mM probenecid. Loading and imaging were performed in Hanks' balanced salt solution (137 mM NaCl, 5.4 mM KCl, 0.4 mM KH_2PO_4, 0.1 mM Na_2HPO_4, 1.3 mM $CaCl_2$, 0.8 mM $MgSO_4$, 5.5 mM glucose, 4 mM $NaHCO_3$, 20 mM HEPES, pH 7.4). Fluorescence intensity at 525 nm was measured at an interval of 1.6 s, using an excitation wavelength of 485 nm and emission cut-off wavelength of 515 nm. 5× agonist 2-APB (0.5 mM) or GSK1016790A (0.5 μM) was added into cell plates at 17 s, and $[Ca^{2+}]_i$ was measured at 140 s.

Structural Modeling—The Rosetta *de novo* modeling method (42) was applied to predict the three-dimensional structure of TRPV4 C terminus residues 838–857. This method has previously been reviewed in detail (43). Briefly, from the Protein Data Bank database, a library of 200 3- and 9-residue fragments was constructed at each of the 20 residues of the target protein. These fragments were then assembled to form the target protein based on the Monte Carlo simulated annealing algorithm. During this process, Rosetta energy functions were used to evaluate the energy of fragment assembly conformations, so at the end of each simulated annealing trajectory, one decoy with the lowest energy was generated. With the Ephiphany high performance computing cluster at the University of California (Davis, CA), 10,000 such decoys were calculated. These decoys were further clustered with a radius of 2 Å. The decoy from the top five largest clusters with the lowest energy was picked as the final model of the target protein.

Statistics—All data are expressed as mean ± S.E. Statistical significance was assessed by Student's *t* test using Prism version 5.0 software. A value of $p < 0.05$ was considered to represent statistical significance.

RESULTS

Identification of a TRPV4 C-terminal Segment Critical for Channel Function—To analyze the role of the C terminus in regulating TRPV4 channel function, we started by generating three progressive deletions (Δ858–871, Δ838–871, and Δ818–871) in which the distal C-terminal 14, 34, and 54 residues, respectively, were removed (Fig. 1*A*). Expression of each construct in HEK293 cells was analyzed by Western blot. As shown in Fig. 1*B*, both wild-type TRPV4 and the mutant with the shortest deletion, TRPV4Δ858–871, showed robust expression with double bands, of which the upper band (slower migration) is typical for proteins in the complex-glycosylated form (29). In contrast, the other two deletion mutants, TRPV4Δ838–871 and TRPV4Δ818–871, showed only one band of the faster migration proteins (Fig. 1*B*), indicating that these two C-terminal deletion mutants did not reach the Golgi for further modification and maturation and hence were trapped in the ER.

To assess the function of the three deletion mutants, we introduced double mutations (N456H and W737R; named TRPV4dm) that rendered TRPV4 sensitive to 2-APB (44), a potent agonist for TRPV1, TRPV2, and TRPV3 but not the wild-type TRPV4 (45). Whole-cell patch clamp recordings confirmed that robust currents from TRPV4dm-expressing cells were observed in the presence of 300 μM 2-APB as well as 0.1 μM TRPV4 specific agonist GSK1016790A, whereas wild-type TRPV4 was activated only by GSK1016790A and not 2-APB (21) (Fig. 1*C*). The 2-APB-induced current exhibited similar outward rectification as the GSK1016790A-induced current but declined rapidly due to desensitization (see also Fig. 1*E*). Currents from both wild-type and TRPV4dm could be completely blocked by application of 130 mM Ba^{2+}, which also blocks TRPV1 current (46) (Fig. 1*C*). These results confirmed that the TRPV4dm channel was fully functional.

To test functional expression of the deletion mutants, we first utilized a FlexStation microplate reader to detect the intracellular calcium level. We found that cells expressing either TRPV4dm or TRPV4dmΔ858–871 channels yielded a robust calcium influx signal in the presence of 2-APB (100 μM) (Fig. 1*D*). In contrast, cells expressing TRPV4dmΔ838–871 or TRPV4dmΔ818–871 did not respond to application of 2-APB, suggesting that residues 838–857 are critical for TRPV4 function. Whole-cell current recordings confirmed that indeed deletion of residues 838–857 in the TRPV4dm background (TRPV4dmΔ838–857) rendered the channel completely irresponsive to 2-APB up to 300 μM (Fig. 1*F*). These results indicate that the C-terminal residues 838–857 of TRPV4 are essential for channel function.

Deletion of Residues 838–857 Causes ER Retention of Channel Proteins—We next investigated how deletion of residues 838–857 eliminates channel current. To examine the role of residues 838–857 in channel trafficking, we tested surface expression of TRPV4dmΔ838–857 using confocal fluorescence microscopy and surface labeling by biotinylation. Confocal images of HEK293 cells co-transfected with TRPV4dm-

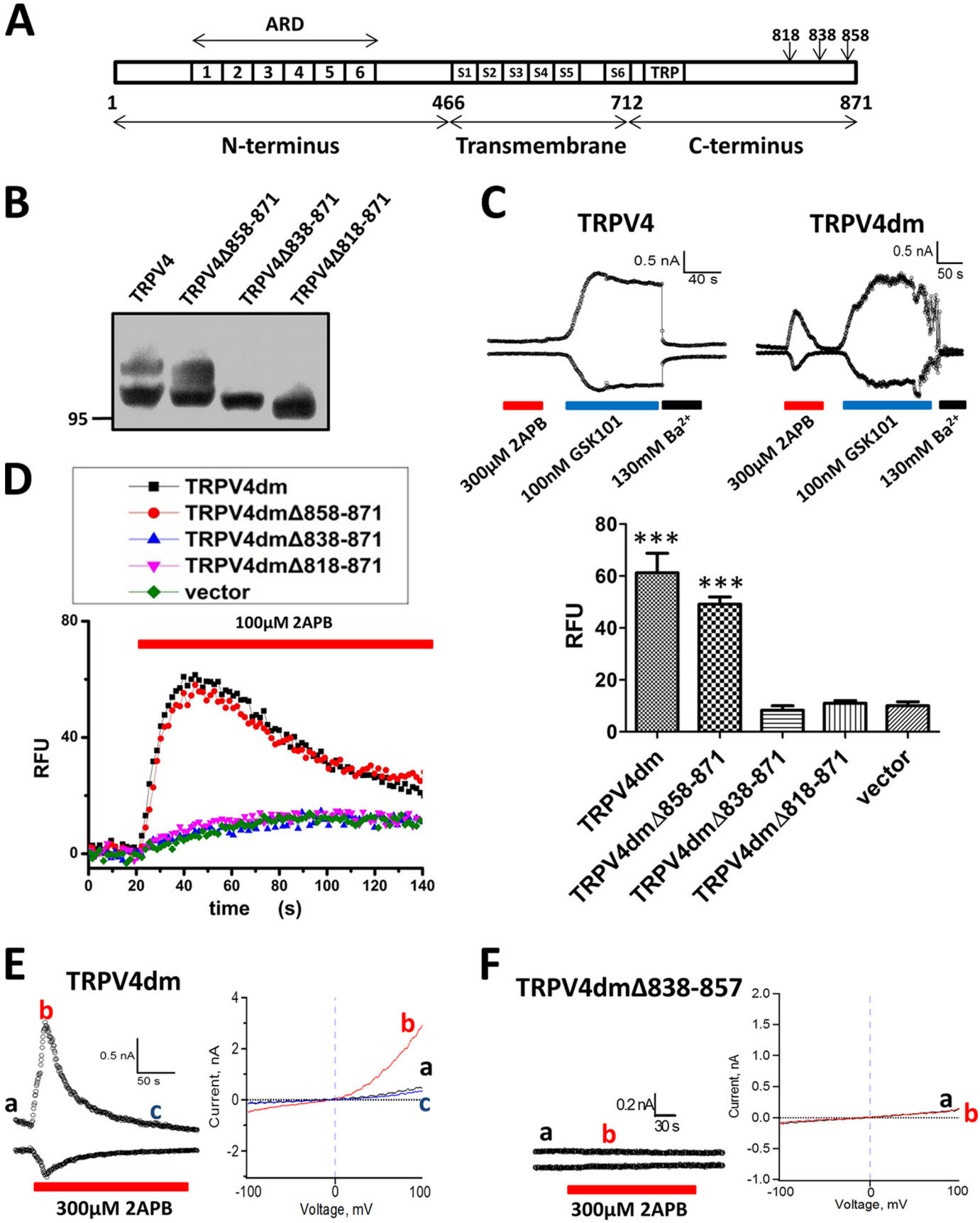

EGFP and an ER marker (DsRed2-ER) showed robust surface expression of TRPV4dm-EGFP, as indicated by strong green fluorescence signals at the cell perimeter that did not overlap with the red fluorescence signals from DsRed2-ER (Fig. 2*A*). In contrast, cells co-transfected with TRPV4dmΔ838–857-EGFP and DsRed2-ER showed co-localization of the two protein constructs, indicating that TRPV4dmΔ838–857 proteins are trapped in the ER (Fig. 2*A*). To quantify the relative levels of surface expression, we used biotin to label TRPV4dm or TRPV4dmΔ838–857 proteins on the cell surface, followed by Western blot analysis. Biotin labeling showed expression of TRPV4dm channel proteins with the typical two bands, of which the slower migrating band probably resulted from glycosylation. In contrast, the expression of both total and surface TRPV4dmΔ838–857 mutant channels was significantly reduced, with a disappearance of the slower migrating upper band (Fig. 2*B*). The result shows that TRPV4dmΔ838–857 channels were not glycosylated, probably due to trapping in the ER, indicating that this may be the reason for the low total protein yield.

To confirm that the upper band proteins indeed resulted from complex glycosylation, we utilized two types of enzyme glycosidase treatments: endoglycosidase H that cleaves *N*-linked high mannose-rich oligosaccharides and peptide:*N*-glycosidase F that cleaves both *N*-linked high mannose-rich oligosaccharides and complex oligosaccharides. As shown in Fig. 2*C*, treatment with peptide:*N*-glycosidase F, but not endoglycosidase H, resulted in disappearance of the slower migrating band for TRPV4dm proteins. TRPV4dmΔ838–857 proteins showed only the faster migrating band, indicating that they were not complex-glycosylated. These results suggest that dysfunctional TRPV4dmΔ838–857 is probably misfolded and retained in the ER.

Accelerated Degradation of TRPV4dmΔ838–857 Mediated by the Proteasomal Pathway—The lack of complex glycosylation suggests that TRPV4dmΔ838–857 channel proteins are trapped in the ER and hence unable to reach Golgi for maturation. To investigate whether TRPV4dmΔ838–857 channels were subject to accelerated degradation, we treated HEK293 cells expressing TRPV4dm or TRPV4dmΔ838–857 with the protein synthesis blocker cycloheximide (CHX) for 8 h and evaluated protein degradation by Western blot (Fig. 3*A*). The half-life of TRPV4dmΔ838–857 was about 4 h, as compared with TRPV4dm with a half-life of more than 8 h (Fig. 3*B*). To further determine whether degradation of TRPV4dmΔ838–857 proteins was mediated by the proteasome or lysosome pathway, the proteasome pathway inhibitor MG132 and the lysosome pathway inhibitor chloroquine were used. As a control, TRPV4dm-expressing cells were treated with CHX and simultaneously added with either MG132 or chloroquine. TRPV4dm showed no significant difference in the rate of protein degradation (Fig. 3*C*). In contrast, the degradation of TRPV4dmΔ838–857 mutant proteins was significantly reversed by MG132, which inhibits the proteasome pathway, but not by chloroquine (Fig. 3*D*). Our results are consistent with TRPV4dmΔ838–857 mutant proteins being primarily degraded by the proteasome-mediated ERAD pathway.

Identification of Two Residues, Gly^{849} and Pro^{851}, Critical for Producing Functional Channels—In order to better understand how residues 838–857 affect protein maturation, we modeled the structure of this short cytoplasmic segment using the Rosetta method, which has been successful in modeling multisubunit channel protein complexes (42, 43), including the TRPV1 channel pore-forming region(47). The *de novo* structural model of residues 838–857 is shown in Fig. 4*A*. There is a well defined α-helix between Val^{843} and Leu^{848}, followed by a sharp turn at Gly^{849}-Asn^{850}. A shorter α-helix, consisting of Pro^{851}–Cys^{853}, was predicted at the distal part. The structure for the rest of the segment appeared to be less defined. Sequence alignments of TRPV4 channels from different species (Fig. 4*B*) revealed that most of the amino acids in the long and short α-helices are well conserved. Similarly, the two residues defining the turn, Gly^{849} and Pro^{851}, both characteristic amino acids in terminating an α-helical region, are conserved. Sequence conservation through evolution at these key positions would contribute to preservation of the overall helix-turn-helix feature of this structural segment, indicating that maintaining the native structure at residues 838–857 is crucial.

To test whether an intact structure of residues 838–857 is required, we generated serial deletion mutants. As shown in Fig. 4*C*, deletion mutant TRPV4dmΔ847–857 resulted in the complete disappearance of complex glycosylation, whereas the mutant with a shorter deletion, TRPV4dmΔ852–857, exhibited some complex glycosylation. This result indicates that the five amino acids, residues 847–851, are critical for complex glycosylation. Indeed, deleting just these five amino acids eliminated the slower migrating band (Fig. 4*C*, TRPV4dmΔ847–851). Simultaneously mutating the two conserved residues Gly^{849} and Pro^{851} to an alanine was sufficient to ablate complex glycosylation, whereas single-point mutation N850A was ineffective (Fig. 4*C*). These results are consistent with the helix-turn-helix structure, confirming that the structural integrity of residues 838–857 is required for producing functional channels.

To further confirm the results described above, we measured calcium influx from cells expressing these mutants. The result showed that both TRPV4dmΔ852–857 and the point mutation TRPV4dmN850A that retained complex glycosylation re-

FIGURE 1. **A TRPV4 C-terminal segment critical for channel function.** *A*, a schematic overview of TRPV4 channels illustrating cytoplasmic N- and C-terminal regions and transmembrane domains (*S1–S6*) and the location of C-terminal deletion mutations (Δ858–871, Δ838–871, and Δ818–871). *B*, Western blot analysis of protein expression of FLAG-tagged TRPV4 and its mutants in HEK293 cells. The molecular mass standard is indicated in kDa on the *left*. *C*, whole-cell currents recorded at +80 and −80 mV from CHO cells expressing WT TRPV4 or TRPV4dm (double mutation of TRPV4 N456H/W737R) in response to the addition of 300 μM 2-APB, 100 nM GSK101, and subsequent block by 130 mM Ba^{2+}. *D*, *left*, fluorescent calcium signals measured over time in response to 100 μM 2-APB for different groups of cells transfected with TRPV4dm (double mutation of TRPV4 N456H/W737R) or its mutants (Δ858–871, Δ838–871, and Δ818–871) or vector as a control. *Right*, histogram shows the average maximum fluorescence intensity. Data are expressed as mean ± S.E. (*error bars*) ($n = 4–6$; ***, $p < 0.001$ *versus* vector control). *E*, *left*, time course of whole-cell currents of TRPV4dm activated by 300 μM 2-APB and measured at voltage steps to +80 and −80 mV from a holding potential of 0 mV. *Right*, *I*-V curves obtained from voltage ramps at time points *a*, *b*, and *c*, as marked on the *left*. *F*, cell expressing the deletion mutant TRPV4dmΔ838–857 does not respond to 2-APB. *RFU*, relative fluorescence units.

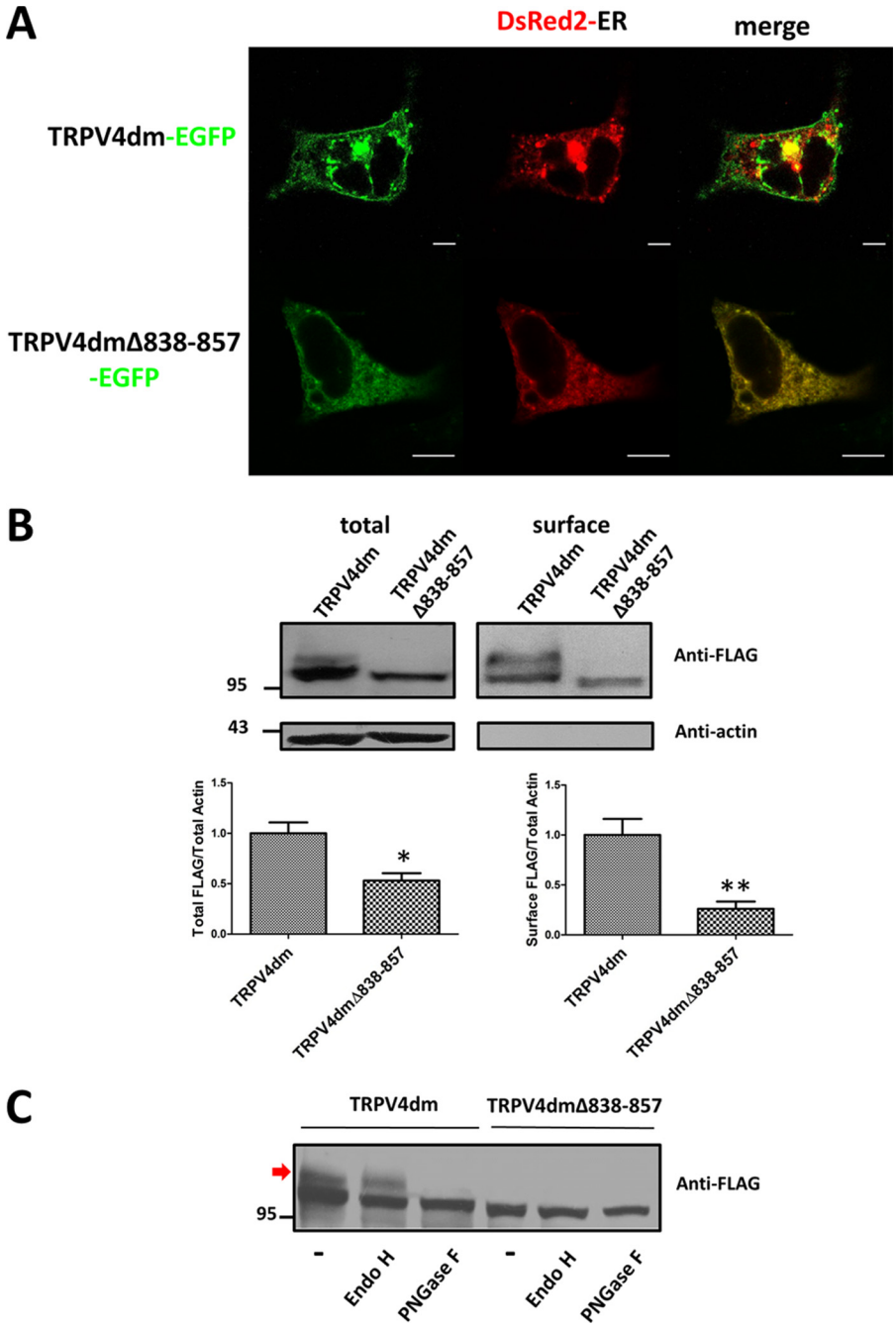

FIGURE 2. **Deletion of residues 838–857 causes ER retention of channel proteins.** *A*, confocal imaging of HEK293 cells co-transfected with either TRPV4dm-EGFP or TRPV4dmΔ838–857-EGFP (*left panels*, *green*) and an ER marker, DsRed2-ER (*middle panels*, *red*) and after merge (*right panels*). *Scale bar*, 10 μm. *B*, total and surface expression of TRPV4dm or TRPV4dmΔ838–857 proteins in transiently transfected HEK293 cells were assessed by biotinylation. In the lower panels, total FLAG-tagged TRPV4dm or TRPV4dmΔ838–857 proteins over actin (*left*) and surface proteins over actin (*right*) were normalized to that of TRPV4dm over actin. Data are expressed as the mean ± S.E. (*error bars*) ($n = 4$; *, $p < 0.05$; **, $p < 0.01$). *C*, glycosylation analysis of TRPV4dm and TRPV4dmΔ838–857 by Western blot. Total proteins (~60 μg) from transiently transfected HEK293 cells were divided into three portions and treated with enzyme endoglycosidase H (*Endo H*) or peptide:*N*-glycosidase F (*PNGase F*) or untreated (−).

sponded to 2-APB treatment (100 μM) with a robust calcium influx signal similar to that seen in TRPV4dm-expressing cells (Fig. 4*D*). In contrast, the complex glycosylation-deficient mutants TRPV4dmΔ847–857, TRPV4dmΔ847–851, and TRPV4dmG849A/P851A were all irresponsive to 2-APB treatment. These results are consistent with results from the protein maturation experiments, suggesting that mutant channels lacking complex glycosylation are not folded properly, thus leading to channel dysfunction.

Functional Rescue of TRPV4 G849A/P851A Mutant by Lowering Temperature—To test the hypothesis that the lack of complex glycosylation and dysfunction of the deletion mutants were caused by protein misfolding, we tested whether lowering temperature could rescue mutant channel function (48, 49). HEK293 cells transfected with either TRPV4dm or TRPV4dmG849A/P851A were incubated at 30 °C for 24–48 h before Western blot analysis. As shown in Fig. 5*A*, lowering the incubation temperature from 37 to

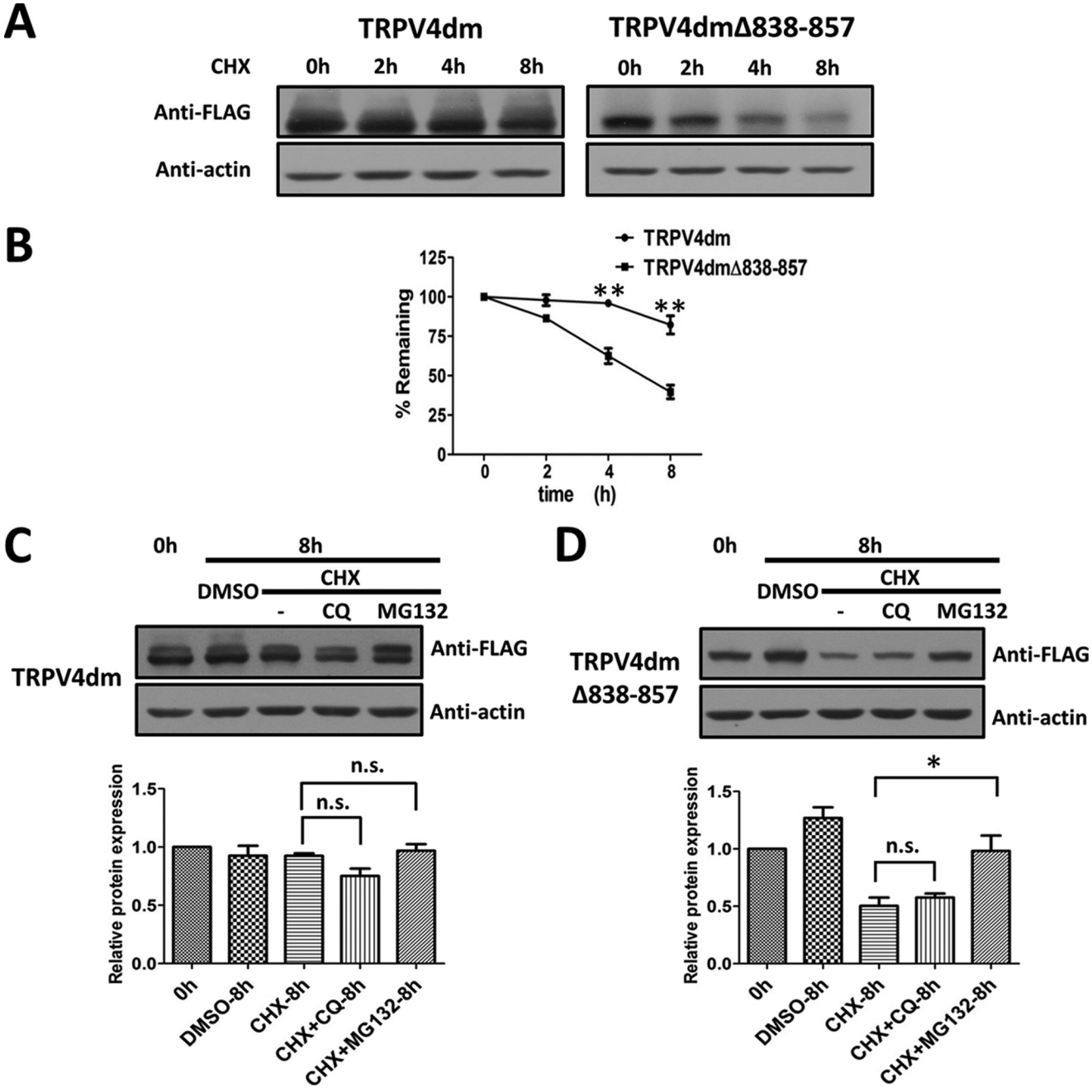

FIGURE 3. **Accelerated degradation of TRPV4dmΔ838–857 mediated by the proteasomal pathway.** *A*, HEK293 cells expressing TRPV4dm (*left*) or TRPV4dmΔ838–857 (*right*) were treated with protein synthesis inhibitor CHX (75 μg/ml) for the indicated time period (0, 2, 4, or 8 h). *B*, the half-life of TRPV4dm degradation was more than 8 h, and the half-life of TRPV4dmΔ838–857 was about 4 h. Data are expressed as the mean ± S.E. (*error bars*) ($n = 3$; **, $p < 0.01$). *C*, Western blotting analysis of TRPV4dm in HEK293 cells treated with CHX (75 μg/ml) and chloroquine (*CQ*; 50 μM) or MG132 (20 μg/ml). Samples were loaded in the following order: control without any treatment, DMSO treatment for 8 h, CHX for 8 h, CHX with chloroquine for 8 h, and CHX with MG132 for 8 h. Data were normalized to that of control without any treatment and expressed as the mean ± S.E. ($n = 3$). *n.s.*, no significance. *D*, degradation of TRPV4dmΔ838–857 mutant proteins was significantly reversed by MG132 but not by chloroquine. Data were normalized to that of control without any treatment and expressed as the mean ± S.E. ($n = 3$; *, $p < 0.05$; *n.s.*, no significance).

30 °C indeed resulted in partial recovery of complex glycosylation for TRPV4dmG849A/P851A.

To test whether channel function was also rescued by lowering the temperature, we recorded both calcium signal and channel current from cells transfected with TRPV4dmG849A/P851A and incubated at 30 °C. In the calcium influx assay, these cells gave rise to a large calcium influx signal in response to 2-APB, whereas cells expressing the vector control yielded a minor change in fluorescence intensity (Fig. 5*B*). Whole-cell current recordings further demonstrated that in the presence of 2-APB, the current of TRPV4dmG849A/P851A was partially rescued by low temperature at 30 °C, as compared with a temperature of 37 °C (Fig. 5, *C* and *D*). To further confirm that the two residues Gly^{849} and Pro^{851} are critical for proper folding, we generated a double mutant, TRPV4G849A/P851A, in the wild typeTRPV4 background that is insensitive to 2-APB but sensitive to GSK1016790A. As shown in Fig. 5, *E* and *F*, when lowering the temperature from 37 to 30 °C, TRPV4G849A/P851A

channels gave rise to a robust increase of the calcium level signal upon application of GSK1016790A, demonstrating the rescue of TRPV4G849A/P851A channel function. These results are consistent with the structural model of residues 838–857, indicating that the two residues Gly[849] and Pro[851] are critical for channel proper folding.

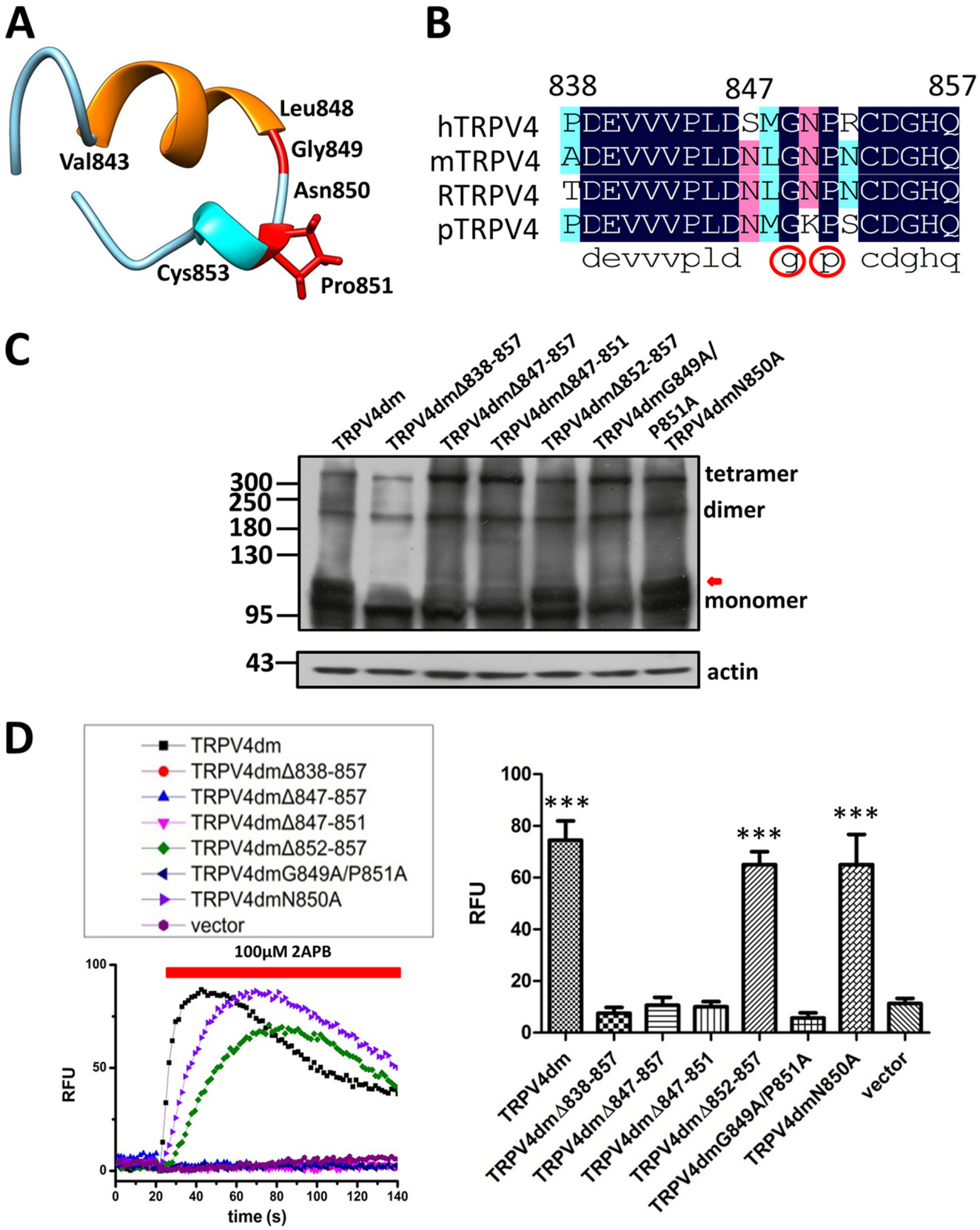

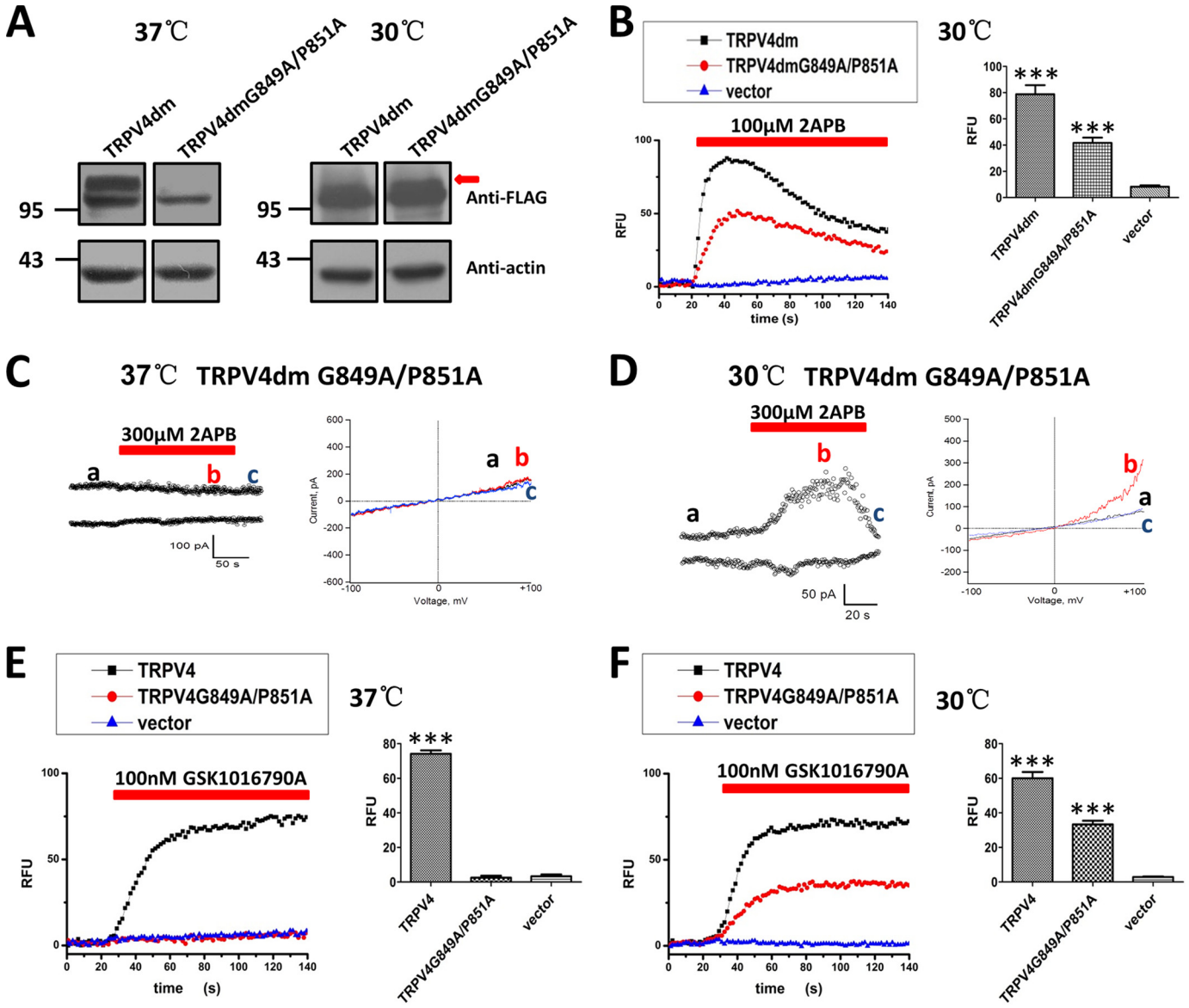

FIGURE 5. **Functional rescue of TRPV4 G849A/P851A mutant by lowering temperature.** *A*, Western blot analysis of protein expression of FLAG-tagged TRPV4dm and TRPV4dmG849A/P851A proteins extracted from cells cultured for 24–36 h at a temperature of 37 and 30 °C, respectively. *B*, *left*, calcium fluorescent traces of TRPVdm and TRPV4dmG849A/P851A were measured in response to 100 μM 2-APB over time from cells cultured for 24–36 h at 30 °C. *Right*, histogram summarizes the average of maximum fluorescence intensities. Data are expressed as the mean ± S.E. (*error bars*) ($n = 4–6$; ***, $p < 0.001$ *versus* vector control). *C*, whole-cell currents recorded from cells expressing TRPV4dmG849A/P851A, cultured for 24–36 h at 37 °C, and activated by 300 μM 2-APB. *a*, *b*, and *c* indicate the time points when current amplitude is measured. *D*, whole-cell currents recorded from cells expressing TRPV4dmG849A/P851A, cultured for 24–36 h 30 °C, and activated by 300 μM 2-APB. *E*, fluorescent calcium signals measured over time in response to 100 nM GSK1016790A, from HEK293 cells transfected with WT TRPV4, TRPV4G849A/P851A, or vector as a control and cultured for 24–36 h at 37 °C. The histogram shows the average of maximum fluorescence intensities. Data are expressed as the mean ± S.E. ($n = 4–6$; ***, $p < 0.001$ *versus* vector control). *F*, fluorescent calcium signals measured over time in response to 100 nM GSK1016790A, from HEK293 cells transfected with WT TRPV4, TRPV4G849A/P851A, or vector as a control and cultured for 24–36 h at 30 °C. *RFU*, relative fluorescence units.

The Segment of Residues 838–857 Mediates C-terminal Interactions—The data above demonstrate that the C terminus plays a critical role in channel folding and maturation. It has been suggested that interactions between intracellular domains mediate TRPV4 channel assembly and trafficking (38). To test whether residues 838–857 participate in interdomain interactions, we used confocal imaging in combination with membrane-tethered peptide Gap43 (growth-associated protein 43), a cytoplasmic protein attached to the membrane by palmitoylation (50). As a positive control, expression of Gap43-tagged

FIGURE 4. **Identification of two residues Gly^{849} and Pro^{851} critical for channel function.** *A*, the *de novo* structural model of residues 838–857. Rosetta modeling predicts a well defined α-helix between Val^{843} and Leu^{848} (*orange*), followed by a sharp turn at Gly^{849}-Asn^{850} (*red*). A shorter α-helix, consisting of Pro^{851} (*red*) to Cys^{853}, is predicted at the distal part (*bright cyan*). Structures for the rest of the segment appeared to be less defined (*cyan*). *B*, sequence alignment of residues 838–857 from human, mouse, rat and pig TRPV4 channels. The two conserved residues Gly^{849} and Pro^{851} are highlighted in *red*. *C*, Western blot analysis of monomer, dimer, and tetramer formation by full-length TRPV4dm and its truncated forms. Complex glycosylation is indicated with a *red arrow*. *D*, *left*, Ca^{2+} fluorescent signals of TRPV4dm or its truncated forms evoked by 100 μM 2-APB over time. *Right*, histogram summarizes the average of maximum fluorescence intensities. Data are expressed as the mean ± S.E. (*error bars*) ($n = 4–6$; ***, $p < 0.001$ *versus* vector control). *RFU*, relative fluorescence units.

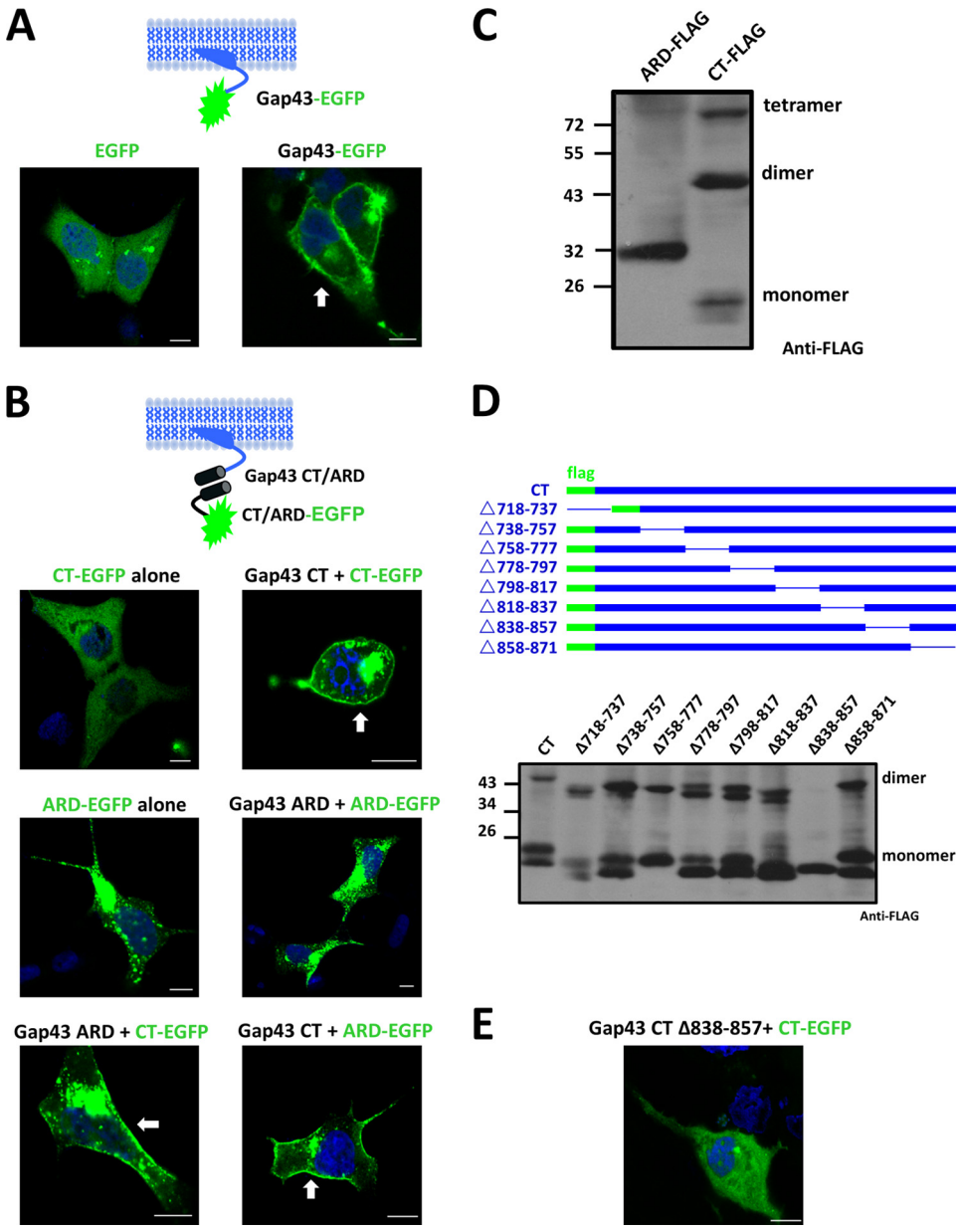

FIGURE 6. **The segment of residues 838–857 mediates C-terminal interactions.** *A*, schematic illustration of the EGFP-tagged peptide Gap43 tethered to the cell membrane. Confocal images show the fluorescence in HEK293 cells transfected with EGFP alone as a control (*left*), or Gap43-EGFP proteins (*right*, *filled white arrow* indicates membrane fluorescence). *Scale bar*, 10 μm. *B*, detection of interaction between the Gap43-fused and free C terminus or ARD. Confocal images show fluorescence from EGFP that is fused to the free C terminus or N-terminal ARD. *Filled white arrows* indicate membrane fluorescence. *Scale bar*, 10 μm. *C*, Western blot analysis under the non-reducing condition demonstrating monomer, dimer, and tetramer formation by FLAG-tagged C terminus but only monomers by ARD. *D*, *top*, schematic representation of TRPV4 C-terminal deletion mutants created for analysis of dimerization. The deleted regions are indicated by *thin blue lines*. The *solid green bars* indicate the FLAG tag fused to the N terminus for Western blot analysis. *Bottom*, Western blot analysis of dimer formation under the non-reducing condition. *E*, Gap43-tagged C terminus lacking residues 838–857 (Gap43 CTΔ838–857) cannot change the distribution of the corresponding full-length EGFP-tagged C terminus. *Scale bar*, 10 μm.

EGFP showed membrane-localized fluorescence in HEK293 cells, as compared with the dispersed expression pattern of free EGFP proteins (Fig. 6*A*), confirming that Gap43 was successfully tethered to the membrane. With this tool, we could detect interactions between isolated N- and/or C-terminal domains because Gap43 would bring the interacting complex to the plasma membrane, as illustrated in Fig. 6*B* (*top*). We observed that, whereas the TRPV4 C terminus tagged with EGFP (CT-EGFP) alone showed a diffused distribution pattern, the membrane-tethered Gap43-CT was capable of tethering the CT-EGFP proteins to the cell surface (Fig. 6*B*, *first row*), indicating that the TRPV4 C terminus can form homomeric interactions. A similar conclusion was reached previously using a cell-free pull-down assay (51). Consistent with results from that study, Gap43-ARD failed to redistribute ARD-EGFP, indicating a lack of interaction between the N termini (Fig. 6*B*, *second row*). A Western blot assay further showed that the N-terminal ARD ran only as monomers, as compared with monomers, dimers, and tetramers for the C terminus (Fig. 6*C*). Interestingly, co-expressing membrane-tethered Gap43-ARD with CT-EGFP resulted in redistribution of fluorescent CT-EGFP to the surface. Similarly, co-expression of membrane-tethered

Gap43-CT with ARD-EGFP also caused ARD-EGFP targeting to the cell surface (Fig. 6*B*, *bottom row*). These results, obtained in live cells, are different from results derived from previous pull-down assays (51), indicating that in the cytosolic environment, the N-terminal ARD and the C terminus can form interdomain complexes.

To assess the role of residues 838–857 in mediating C-terminal homomeric interaction, we made a series of deletions within the C terminus (Fig. 6*D*, *top*). We used Western blot under non-reducing conditions to detect homodimeric interaction between the deletion mutants. The CT, as a positive control, showed clear dimer formation. Although truncation of the C-terminal residues 838–857 led to a loss of dimer formation, other deletion mutants retained the ability to form dimers (Fig. 6*D*, *bottom*). Consistent with the in-solution experiments, tests in live cells showed that the Gap43-tagged C terminus without residues 838–857 (Gap43 CTΔ838–857) could not alter the distribution of the EGFP-tagged C terminus (Fig. 6*E*). These data suggest that residues 838–857 play a crucial role in mediating oligomerization between the C termini of TRPV4.

DISCUSSION

In the present study, our objective was to elucidate the role of the TRPV4 C terminus in regulating channel activity because mutations in intracellular regions are known to cause human diseases as a result of altered channel activity. Using a combination of biochemical approaches, confocal imaging, calcium influx assay, and electrophysiology, we identified a novel narrow region in the C terminus of TRPV4 whose disruption ablates channel activity. We propose that the lack of channel activity is due to mutational effects on protein folding. Misfolded mutant proteins are trapped in the ER and fail to reach Golgi, where complex glycosylation takes place, for maturation, thus leading to accelerated ER-associated degradation through the proteasomal pathway. This conclusion was based on multiple lines of experimental evidence. First, serial C-terminal deletions revealed a critical segment consisting of residues 838–857. By introducing the 2-APB activation site to the otherwise insensitive TRPV4, we were able to demonstrate with both calcium imaging and whole-cell patch clamp recordings that TRPV4dmΔ838–857 is not functional. Second, results from confocal imaging and surface labeling indicated that the majority of TRPV4dmΔ838–857 proteins were trapped in the ER, which led to accelerated degradation of the mutant proteins through the proteasomal ERAD pathway. Third, structural analysis suggested that residues 838–857 probably adopt a helix-turn-helix conformation. Point mutations of Gly^{849} and Pro^{851} at the turn are expected to destabilize or even disrupt this conformation. Indeed, point mutations G849A/P851A exhibited a similar effect on trafficking and protein maturation as the deletion mutation Δ838–857. Furthermore, lowering the incubation temperature from 37 to 30 °C can significantly increase the channel complex glycosylation and 2-APB-induced calcium influx for TRPV4dmG849A/P851A. Therefore, we propose that C-terminal residues 838–857 of TRPV4 function as a folding recognition domain. Native conformation of this domain ensures channel protein maturation and surface targeting, whereas misfolding of this domain hinders protein maturation. Although a small fraction of improperly processed channel proteins may escape the normal ER-Golgi-surface membrane pathway and target to the plasma membrane through a Golgi-independent pathway (52), results from the present study indicate that they cannot form functional channels. Destabilization of the folding recognition domain through mutations or pharmacological intervention thus would be expected to counter the overactive phenotype seen in skeletal dysplasias caused by TRPV4 genetic mutations.

Residues Gly^{849} and Pro^{851} within the proposed folding recognition domain of TRPV4 are well conserved among homeothermic (warm blood) species. Alanine substitutions of only these two residues exert similar effects, seen by more severe deletion mutations of this domain, whereas a single-point mutation, N850A, has no undetectable effect on channel function. The Rosetta-based structure model, although tentative due to the nature of *de novo* structure prediction, provides hints on how this may come about. We propose that mutational effects are probably results of disruption of the conformation of this region required for the normal protein maturation process. Rescue of TRPV4 G849A/P851A channel function by lowering incubation temperature is fully consistent with this hypothesis, indicating that misfolding is probably the cause for ER retention and loss of function, as previously documented in other misfolding proteins (30, 48, 49). Given that segment deletions within a broad neighboring region of the C terminus were tolerable, results from the present study are best explained by a working model assuming that the region around residues of Gly^{849} and Pro^{851} is essential for correct folding of the TRPV4 channel.

The cytosolic C terminus of TRPV4 harbors many binding sites for various interacting proteins and factors, such as F-actin, tubulin, MAP7, inositol trisphosphate receptor, and calmodulin, that are relevant to regulation of subunit assembly, trafficking to the plasma membrane, and channel activity (33, 34, 36, 37). It is of interest to note that the proposed C-terminal folding recognition domain turns out to overlap with the calmodulin-binding site previously shown to induce conformational changes and Ca^{2+}-dependent potentiation of TRPV4 (36, 53). Calmodulin binding to the C terminus, in response to rises in intracellular Ca^{2+} following extensive channel activity, displaces its interaction with an N-terminal domain (residues 117–136) of the same subunit (54). Our results from live cell confocal fluorescence imaging of membrane-tethered Gap43 show that the N-terminal ARD (residues 149–394) of TRPV4 can also interact with the C terminus. In addition, intersubunit interactions can be mediated by homodimeric formation between C termini. Therefore, the proposed folding recognition domain may play a crucial role in both channel protein maturation and dynamic regulation of channel activity.

Glycosylation characterizes the maturation process of TRPV4 proteins, from the *N*-linked high mannose glycosylation form in the ER to the complex glycosylation form in the Golgi apparatus, before targeting to the cell surface membrane, where they carry out their transmembrane ion transport function. The absence of complex glycosylation is manifested by the deletion of residues 838–857, indicating that mutant channels are trapped in the ER and fail to reach the Golgi apparatus.

Misfolded TRPV4 proteins are probably retained by the ER-associated proteins, such as OS-9 (55); alternatively, "cargo receptors" present at the ER exit sites may fail to recognize misfolded TRPV4Δ838–857 (56). A previous study demonstrated that deletion of C-terminal residues 828–856 inhibits TRPV4 trafficking and causes ER retention (38). Our present study confirms the earlier report and provides a mechanistic framework for understanding the mutational effects and channel function. Interestingly, we demonstrate that, although mutations to the proposed folding recognition domain prevented protein complex glycosylation, some of the mutant proteins could still reach the surface membrane (*e.g.* see Fig. 2*B*); these unprocessed proteins are unable to form functional channels, however, as demonstrated by calcium imaging and patch clamping recordings. Similarly, it is observed that channels with a deletion of residues 828–856 could be exported upon coexpression with full-length TRPV4 (38). Observations of dimer and tetramer formation of deletion mutants (*e.g.* see Fig. 4*C*) imply that other parts of the channel protein also participate in mediating subunit-subunit interactions. Indeed, TRPV4 subunits engage in extensive protein-protein interactions over a large surface area within both the membrane-spanning region and cytoplasmic domains (39). Details of these interactions remain to be investigated.

In conclusion, our results provide evidence that the C terminus of TRPV4 is critical for the formation of functional channels. Deletions and mutations of residues 838–837 in the C terminus result in channel proteins being trapped in the ER and become dysfunctional. Our data suggest that targeting the proposed C-terminal folding recognition domain by pharmacological intervention may achieve selective down-regulation of TRPV4 channel activity for therapeutic purposes to treat overactive TRPV4-mediated diseases, such as pain and skeletal dysplasias (23, 26, 57).

Acknowledgments—We thank our laboratory members Feng Zhang, Ningning Wei, Xiling Bian, and Linlin Ma for discussion. K. W. W. thanks J. M. Wang for consistent support during this research.

REFERENCES

1. Ye, L., Kleiner, S., Wu, J., Sah, R., Gupta, R. K., Banks, A. S., Cohen, P., Khandekar, M. J., Boström, P., Mepani, R. J., Laznik, D., Kamenecka, T. M., Song, X., Liedtke, W., Mootha, V. K., Puigserver, P., Griffin, P. R., Clapham, D. E., and Spiegelman, B. M. (2012) TRPV4 is a regulator of adipose oxidative metabolism, inflammation, and energy homeostasis. *Cell* **151,** 96–110
2. Liedtke, W., Choe, Y., Martí-Renom, M. A., Bell, A. M., Denis, C. S., Sali, A., Hudspeth, A. J., Friedman, J. M., and Heller, S. (2000) Vanilloid receptor-related osmotically activated channel (VR-OAC), a candidate vertebrate osmoreceptor. *Cell* **103,** 525–535
3. Strotmann, R., Harteneck, C., Nunnenmacher, K., Schultz, G., and Plant, T. D. (2000) OTRPC4, a nonselective cation channel that confers sensitivity to extracellular osmolarity. *Nat. Cell Biol.* **2,** 695–702
4. Hille, B. (2001) *Ion Channels of Excitable Membranes*, 3rd Ed., pp. 131–135, Sinauer Associates, Inc., Sunderland, MA
5. Clapham, D. E. (2003) TRP channels as cellular sensors. *Nature* **426,** 517–524
6. Venkatachalam, K., and Montell, C. (2007) TRP channels. *Annu. Rev. Biochem.* **76,** 387–417
7. Montell, C. (2001) Physiology, phylogeny, and functions of the TRP superfamily of cation channels. *Sci. STKE 2001*, re1
8. Saito, S., and Shingai, R. (2006) Evolution of thermoTRP ion channel homologs in vertebrates. *Physiol. Genomics* **27,** 219–230
9. Shigematsu, H., Sokabe, T., Danev, R., Tominaga, M., and Nagayama, K. (2010) A 3.5-nm structure of rat TRPV4 cation channel revealed by Zernike phase-contrast cryoelectron microscopy. *J. Biol. Chem.* **285,** 11210–11218
10. Loukin, S., Su, Z., and Kung, C. (2011) Increased basal activity is a key determinant in the severity of human skeletal dysplasia caused by TRPV4 mutations. *PLoS One* **6,** e19533
11. Andreucci, E., Aftimos, S., Alcausin, M., Haan, E., Hunter, W., Kannu, P., Kerr, B., McGillivray, G., McKinlay Gardner, R. J., Patricelli, M. G., Sillence, D., Thompson, E., Zacharin, M., Zankl, A., Lamándé, S. R., and Savarirayan, R. (2011) TRPV4 related skeletal dysplasias. A phenotypic spectrum highlighted byclinical, radiographic, and molecular studies in 21 new families. *Orphanet. J. Rare Dis.* **6,** 37
12. Krakow, D., Vriens, J., Camacho, N., Luong, P., Deixler, H., Funari, T. L., Bacino, C. A., Irons, M. B., Holm, I. A., Sadler, L., Okenfuss, E. B., Janssens, A., Voets, T., Rimoin, D. L., Lachman, R. S., Nilius, B., and Cohn, D. H. (2009) Mutations in the gene encoding the calcium-permeable ion channel TRPV4 produce spondylometaphyseal dysplasia, Kozlowski type and metatropic dysplasia. *Am. J. Hum. Genet.* **84,** 307–315
13. Caterina, M., Güler, A. D., Lee, H., Iida, T., Shimizu, I., and Tominaga, M. (2002) Heat-evoked activation of the ion channel, TRPV4. *J. Neurosci.* **22,** 6408–6414
14. Mendoza, S. A., Fang, J., Gutterman, D. D., Wilcox, D. A., Bubolz, A. H., Li, R., Suzuki, M., and Zhang, D. X. (2010) TRPV4-mediated endothelial Ca^{2+} influx and vasodilation in response to shear stress. *Am. J. Physiol. Heart Circ. Physiol.* **298,** H466–H476
15. Gao, X., Wu, L., and O'Neil, R. G. (2003) Temperature-modulated diversity of TRPV4 channel gating. Activation by physical stresses and phorbol ester derivatives through protein kinase C-dependent and -independent pathways. *J. Biol. Chem.* **278,** 27129–27137
16. Suzuki, M., Mizuno, A., Kodaira, K., and Imai, M. (2002) Impaired pressure sensation in mice lacking TRPV4. *J. Biol. Chem.* **278,** 22664–22668
17. Zheng, J. (2013) Molecular mechanism of TRP channels. *Compr. Physiol.* **3,** 221–242
18. Vriens, J., Watanabe, H., Janssens, A., Droogmans, G., Voets, T., and Nilius, B. (2004) Cell swelling, heat, and chemical agonists use distinct pathways for the activation of the cation channel TRPV4. *Proc. Natl. Acad. Sci. U.S.A.* **101,** 396–401
19. Watanabe, H., Vriens, J., Prenen, J., Droogmans, G., Voets, T., Nilius, B. (2003) Anandamide and arachidonic acid use epoxyeicosatrienoic acids to activate TRPV4 channels. *Nature* **424,** 434–438
20. Watanabe, H., Davis, J. B., Smart, D., Jerman, J. C., Smith, G. D., Hayes, P., Vriens, J., Cairns, W., Wissenbach, U., Prenen, J., Flockerzi, V., Droogmans, G., Benham, C. D., and Nilius, B. (2002) Activation of TRPV4 channels (hVRL-2/mTRP12) by phorbol derivatives. *J. Biol. Chem.* **277,** 13569–13577
21. Thorneloe, K. S., Sulpizio, A. C., Lin, Z., Figueroa, D. J., Clouse, A. K., McCafferty, G. P., Chendrimada, T. P., Lashinger, E. S., Gordon, E., Evans, L., Misajet, B. A., Demarini, D. J., Nation, J. H., Casillas, L. N., Marquis, R. W., Votta, B. J., Sheardown, S. A., Xu, X., Brooks, D. P., Laping, N. J., and Westfall, T. D. (2008) *N*-((1S)-1-{[4-((2S)-2-{[(2,4-dichlorophenyl)-sulfonyl]amino}-3-hydroxypropanoyl)-1-piperazinyl]carbonyl}-3-methylbutyl)-1-benzothiophene-2-carboxamide (GSK1016790A), a novel and potent transient receptor potential vanilloid 4 channel agonist induces urinary bladder contraction and hyperactivity. Part I. *J. Pharmacol. Exp. Ther.* **326,** 432–442
22. Montell, C. (2005) The TRP superfamily of cation channels. *Science's STKE 2005*, re3
23. Everaerts, W., Nilius, B., and Owsianik, G. (2010) The vanilloid transient receptor potential channel TRPV4. From structure to disease. *Prog. Biophys. Mol. Biol.* **103,** 2–17
24. Liedtke, W., Tobin, D. M., Bargmann, C. I., and Friedman, J. M. (2003) Mammalian TRPV4 (VR-OAC) directs behavioral responses to osmotic and mechanical stimuli in *Caenorhabditis elegans*. *Proc. Natl. Acad. Sci. U.S.A.* **100,** 14531–14536
25. Casas, S., Novials, A., Reimann, F., Gomis, R., and Gribble, F. M. (2008)

Calcium elevation in mouse pancreatic β cells evoked by extracellular human islet amyloid polypeptide involves activation of the mechanosensitive ion channel TRPV4. *Diabetologia* **51,** 2252–2262
26. Brierley, S. M., Page, A. J., Hughes, P. A., Adam, B., Liebregts, T., Cooper, N. J., Holtmann, G., Liedtke, W., and Blackshaw, L. A. (2008) Selective role for TRPV4 ion channels in visceral sensory pathways. *Gastroenterology* **134,** 2059–2069
27. Alvarez, D. F., King, J. A., Weber, D., Addison, E., Liedtke, W., Townsley, M. I. (2006) Transient receptor potential vanilloid 4-mediated disruption of the alveolar septal barrier. A novel mechanism of acute lung injury. *Circ. Res.* **99,** 988–995
28. Yin, J., Hoffmann, J., Kaestle, S. M., Neye, N., Wang, L., Baeurle, J., Liedtke, W., Wu, S., Kuppe, H., Pries, A. R., and Kuebler, W. M. (2008) Negative-feedback loop attenuates hydrostatic lung edema via a cGMP-dependent regulation of transient receptor potential vanilloid 4. *Circ. Res.* **102,** 966–974
29. Valverde, M. A., Arniges, M., Fernández-Fernández, J. M., Albrecht, N., and Schaefer, M. (2006) Human TRPV4 channel splice variants revealed a key role of ankyrin domains in multimerization and trafficking. *J. Biol. Chem.* **281,** 1580–1586
30. de Groot, T., van der Hagen, E. A., Verkaart, S., te Boekhorst, V. A., Bindels, R. J., and Hoenderop, J. G. (2011) Role of the transient receptor potential vanilloid 5 (TRPV5) protein N terminus in channel activity, tetramerization, and trafficking. *J. Biol. Chem.* **286,** 32132–32139
31. Tsuruda, P. R., Julius, D., and Minor, D. L. (2006) Coiled coils direct assembly of a cold-activated TRP channel. *Neuron* **51,** 201–212
32. Al-Ansary, D. M., Wissenbach, U., Wagner, T. F., Flockerzi, V., Niemeyer, B. A., and Erler, I. (2006) Trafficking and assembly of the cold-sensitive TRPM8 channel. *J. Biol. Chem.* **281,** 38396–38404
33. Garcia-Elias, A., Lorenzo, I. M., Vicente, R., and Valverde, M. A. (2008) IP3 receptor binds to and sensitizes TRPV4 channel to osmotic stimuli via a calmodulin-binding site. *J. Biol. Chem.* **283,** 31284–31288
34. Suzuki, M., Hirao, A., and Mizuno, A. (2003) Microtubule-associated protein 7 increases the membrane expression of transient receptor potential vanilloid 4 (TRPV4). *J. Biol. Chem.* **278,** 51448–51453
35. Kuehn, E. W., Köttgen, M., Buchholz, B., Garcia-Gonzalez, M. A., Kotsis, F., Fu, X., Doerken, M., Boehlke, C., Steffl, D., Tauber, R., Wegierski, T., Nitschke, R., Suzuki, M., Kramer-Zucker, A., Germino, G. G., Watnick, T., Prenen, J., Nilius, B., and Walz, G. (2008) TRPP2 and TRPV4 form a polymodal sensory channel complex. *J. Cell Biol.* **182,** 437–447
36. Strotmann, R., Schultz, G., and Plant, T. D. (2003) Ca^{2+}-dependent potentiation of the nonselective cation channel TRPV4 is mediated by a C-terminal calmodulin binding site. *J. Biol. Chem.* **278,** 26541–26549
37. Ramadass, R., Becker, D., Jendrach, M., and Bereiter-Hahn, J. (2007) Spectrally and spatially resolved fluorescence lifetime imaging in living cells. TRPV4-microfilament interactions. *Arch. Biochem. Biophys.* **463,** 27–36
38. Jendrach, M., Becker, D., Müller, M., and Leuner, K. (2008) The C-terminal domain of TRPV4 is essential for plasma membrane localization. *Mol. Membr. Biol.* **25,** 139–151
39. Hellwig, N., Albrecht, N., Harteneck, C., Schultz, G., Schaefer, M. (2005) Homo- and heteromeric assembly of TRPV channel subunits. *J. Cell Sci.* **118,** 917–928
40. Alessandri-Haber, N., Joseph, E., Dina, O. A., Liedtke, W., Levine, J. D. (2005) TRPV4 mediates pain-related behavior induced by mild hypertonic stimuli in the presence of inflammatory mediator. *Pain* **118,** 70–79
41. Alessandri-Haber, N., Dina, O. A., Joseph, E. K., Reichling, D. B., and Levine, J. D. (2008) Interaction of transient receptor potential vanilloid 4, integrin, and SRC tyrosine kinase in mechanical hyperalgesia. *J. Neurosci.* **28,** 1046–1057
42. Simons, K. T., Kooperberg, C., Huang, E., and Baker, D. (1997) Assembly of protein tertiary structures from fragments with similar local sequences using simulated annealing and Bayesian scoring functions. *J. Mol. Biol.* **268,** 209–225
43. Rohl, C. A., Strauss, C. E., Misura, K. M., and Baker, D. (2004) Protein structure prediction using Rosetta. *Methods Enzymol.* **383,** 66–93
44. Hu, H., Grandl, J., Bandell, M., Petrus, M., and Patapoutian, A. (2009) Two amino acid residues determine 2-APB sensitivity of the ion channels TRPV3 and TRPV4. *Proc. Natl. Acad. Sci. U.S.A.* **106,** 1626–1631
45. Hu, H. Z., Gu, Q., Wang, C., Colton, C. K., Tang, J., Kinoshita-Kawada, M., Lee, L. Y., Wood, J. D., and Zhu, M. X. (2004) 2-Aminoethoxydiphenyl borate is a common activator of TRPV1, TRPV2, and TRPV3. *J. Biol. Chem.* **279,** 35741–35748
46. Yang, F., Cui, Y., Wang, K., and Zheng, J. (2010) Thermosensitive TRP channel pore turret is part of the temperature activation pathway. *Proc. Natl. Acad. Sci. U.S.A.* **107,** 7083–7088
47. Cui, Y., Yang, F., Cao, X., Yarov-Yarovoy, V., Wang, K., and Zheng, J. (2012) Selective disruption of high sensitivity heat activation but not capsaicin activation of TRPV1 channels by pore turret mutations. *J. Gen. Physiol.* **139,** 273–283
48. Wang, X., Koulov, A. V., Kellner, W. A., Riordan, J. R., and Balch, W. E. (2008) Chemical and biological folding contribute to temperature-sensitive ΔF508 CFTR trafficking. *Traffic* **9,** 1878–1893
49. Harley, C. A., Jesus, C. S., Carvalho, R., Brito, R. M., and Morais-Cabral, J. H. (2012) Changes in channel trafficking and protein stability caused by LQT2 mutations in the PAS domain of the HERG channel. *Plos One* **7,** e32654
50. Benowitz, L. I., and Routtenberg, A. (1997) GAP-43. An intrinsic determinant of neuronal development and plasticity. *Trends Neurosci.* **20,** 84–91
51. Zhang, F., Liu, S., Yang, F., Zheng, J., and Wang, K. (2011) Identification of a tetrameric assembly domain in the C terminus of heat-activated TRPV1 channels. *J. Biol. Chem.* **286,** 15308–15316
52. Nickel, W., and Seedorf, M. (2008) Unconventional mechanisms of protein transport to the cell surface of eukaryotic cells. *Annu. Rev. Cell Dev. Biol.* **24,** 287–308
53. Nilius, B., Vriens, J., Prenen, J., Droogmans, G., and Voets, T. (2004) TRPV4 calcium entry channel. A paradigm for gating diversity. *Am. J. Physiol. Cell Physiol.* **286,** C195–C205
54. Strotmann, R., Semtner, M., Kepura, F., Plant, T. D., and Schöneberg, T. (2010) Interdomain interactions control Ca^{2+}-dependent potentiation in the cation channel TRPV4. *PLoS One* **5,** e10580
55. Wegierski, T., Wang, Y., Fu, X., Gaiser, S., Köttgen, M., Kramer-Zucker, A., and Walz, G. (2007) OS-9 regulates the transit and polyubiquitination of TRPV4 in the endoplasmic reticulum. *J. Biol. Chem.* **282,** 36561–36570
56. Ellgaard, L., and Helenius, A. (2003) Quality control in the endoplasmic reticulum. *Nat. Rev. Mol. Cell Biol.* **4,** 181–191
57. Blackshaw, L. A., Brierley, S. M., and Hughes, P. A. (2010) TRP channels. New targets for visceral pain. *Gut* **59,** 126–135